



Project no.043386

TRIGS

TRIGGERING INSTABILITIES IN MATERIALS AND GEOSYSTEMS

[HTTP://WWW.TRIGS.EU](http://www.trigs.eu)

Sixth Framework Programme (FP6)

**New and Emerging Science and Technology Pathfinder Initiative
(NEST Pathfinder Priority)**

Deliverable n. 1.7.2

**Synthesis report on the comparison between earthquake-triggered landslides and seismic
aftershocks triggered by 5 earthquakes.**

Due date of deliverable: 31/1/2010

Actual submission date: 31/1/2010

Start date of project: 01/2007

Duration: 36 months

Organization name of lead contractor for this deliverable: UJF

Diffusion Level: PU

D1.7.2. Synthesis report on the comparison between catalogs of landslides and earthquakes and implication for the triggering mechanism

Author: L Tatard and J R Grasso (UJF)

Introduction

The triggering of seismic aftershocks in space and time is not well understood and there is still some controversy in seismology about the relative importance of static stress changes (e.g. Stein 1999) versus dynamic stress changes (e.g. Gomberg et al 2003, Johnston and Jia 2005). To our knowledge, only the dynamic triggering has been explored for landslides triggered by earthquakes. Several authors showed that the intensity of landsliding (number of landslides, area affected by landslides, total volume of landslides, maximum distance between earthquake and landslide) scales with earthquake magnitude, as reviewed by Keefer (2002). Here we study the frequency-distance distributions of five landslide and aftershock crises triggered by five 5.5 earthquakes with moment magnitude $M_w > 5.5$. We compare i) the landslide distance distributions with their aftershock distance distribution counterparts and ii) the 5 landslide - aftershock pairs with each other. We then compare the landslide and aftershock distance distributions to the Peak Ground Acceleration, Peak Ground Velocity and Peak Ground Distance distributions for the Northridge and Chi-Chi earthquakes.

Data

We compare earthquake aftershock spatial distributions with landslide spatial distributions triggered by the Chi-Chi $M_w 7.6$ earthquake (Taiwan), by the $M_w 7.6$ Kashmir earthquake (Pakistan), by the $M_w 7.2$ Fiordland earthquake (New Zealand), by the $M_w 6.6$ Northridge earthquake (California) and by the $M_w 5.6$ Rotoehu earthquake (New Zealand). Three criteria, were used for the selection of aftershocks in time, space, and size. In time, aftershocks are selected up to three days after the mainshock, in order to limit aftershock cascading. Besides, it corresponds to the time interval in which most earthquake-triggered landslides fail and therefore allow comparison between landslides and aftershocks. In space, aftershocks are selected within 10 times the ruptured fault length L (using the relation of Wells and Coppersmith (1994) to estimate L as a function of magnitude) as it corresponds to the average maximum distances where mainshocks are found to trigger aftershocks (e.g. Felzer and Brodsky, 2006). In magnitude, we select aftershocks with magnitudes larger than the magnitude of completeness M_c of the aftershock sequence, calculated thanks to the method of Ogata and Katsura (1993).

Results

The hanging wall bears most landslides and aftershocks, if not all, for the five sequences. The actual or inferred surface fault is an efficient boundary delimitating landslide and aftershock occurrences in space. There is a good overlap of the landslide distance distributions to their aftershock distance distribution counterparts, for all five sequences (Figs 1 and 2). This result is robust whatever the type of distance distribution we choose (to hypocenter, to epicenter, to fault surface projection, to actual or inferred surface fault trace). The differences in geologic setting and mainshock characteristics do not influence the overlap between each landslide and aftershock distance distribution pairs. Still, there are second order differences between those five pairs. In the near field, i.e. for distances less than one time the ruptured fault length, we find large differences

between the landslide and aftershock distributions for the Fiordland and Northridge sequences (Figures 1 and 2). These differences primarily arise from the mainshock locations: offshore for the Fiordland sequence, in a plain for the Northridge sequence, where no landslide can occur. In addition, aftershocks are found to be triggered farther away than landslides for the Chi-Chi and Kashmir events. For the 3 other sequences, we observe that, on average, landslides are triggered farther away than aftershocks.

When comparing landslide and aftershock distances to surface fault for the five sequences (Figs 1 and 2), we observe

- an increase for small distances followed by a decrease of events with distance (Fiordland, Northridge, Rotoehu);

- a plateau followed by a decrease (Chi-Chi) or

- a decrease of the number of events with distance (Kashmir).

The exponent values controlling the asymptotic decay varies from one (Kashmir events) to three or larger for most events.

In order to remove the local effects, which possibly modify the differences between the five sequences, we restrict our analysis to events occurring on the hanging wall, bounded to the width of the ruptured fault length. There are no major differences in the distance distributions when using all events or the events restricted to the hanging wall and therefore the specificities for each sequence are kept.

We then check the influence of the mainshock magnitude by normalizing the distances by the earthquake dimension, i.e. the ruptured fault length L (Figs 3b and 4b). For small mainshocks with $M_w < 7.5$, the distribution of aftershocks and landslides as a function of distance show a peak at a distance of the order of the mainshock rupture length. However, the two $M_w 7.6$ mainshocks trigger landslides and aftershocks at much shorter distances than expected from their magnitude. Their landslide and aftershock distributions are different from those observed for the smaller mainshocks. We perform the same scaling on the distance distributions of events situated on the hanging wall, within the width of the ruptured fault length, and retrieve the same results.

Ground motions and triggered landslide and aftershock space distributions

We compare landslide and aftershock distributions to ground motion observations (Peak Ground Acceleration, PGA; Peak Ground Velocity, PGV; Peak Ground Displacement, PGD) for the Chi-Chi and the Northridge sequences. For distances smaller than $0.5L$ (Chi-Chi sequence) and 1 (Northridge sequence), we observe a continuous decrease of the PGA with distance ChiChi, and for Northridge. The PGD decreases with distance for Northridge, but increases with distance for Chichi for distances smaller than $0.5L$. For these distances, the number of landslides and aftershocks increase with distance for both the Chi-Chi and Northridge sequences (Fig. 5). For distances larger than $0.5L$ (Chi-Chi sequence) and 1 (Northridge sequence), we find a continuous decrease of the Chi-Chi and Northridge PGA, PGV and PGD as well as a continuous decrease of the landslide and aftershock distance distributions. The exponent values controlling the asymptotic decay are different for ground motion observations and landslide and aftershock distance distributions, except for the Chi-Chi PGD and the Chi-Chi landslide and aftershock distributions (Fig. 5). Hence the Chi-Chi PGD is the parameter presenting the best qualitative fit to both the Chi-Chi landslide and aftershock distance distributions.

Discussion

Landslide distance distributions display similar patterns as aftershocks, for the five sequences. This result is robust whatever the type of distribution chosen: to hypocenter, to epicenter, to surface projection of the fault, to actual or inferred surface fault trace and for both events or events on the hanging wall, bounded to the width of the ruptured fault length. We suggest that landslide and aftershock triggering is driven by the same mechanisms, ie dynamic and static stress changes. For most landslide and aftershock distance distributions, we retrieved asymptotic decays presenting an exponent larger than 3. The exponent values do not favor either dynamic triggering (theoretical exponent equal to 1) or static triggering (theoretical exponent equal to 2).

As dynamic triggering is the mechanism responsible for large distance aftershock triggering (e.g. Felzer and Brodsky, 2006) and aftershocks were triggered further away than landslides for the five sequences, we can deduce that dynamic triggering is more efficient in triggering aftershocks than landslides. Note that we checked that topography was available for triggering landslides in the same areas where the larger distance aftershocks were triggered. However, landslides which occur far away from the epicenter could have been missed during the landslide reconnaissances and future reconnaissances after large earthquakes should encompass distances at least as far as ten times the ruptured fault length (the distance up to which aftershocks are known to be triggered, e.g. Felzer and Brodsky, 2006).

The near field behavior between aftershock and landslide distance distributions is either roughly similar or strongly influenced by the available topography. Therefore we cannot deduce from near-field specificities any difference in landslide and aftershock triggering.

Each landslide - aftershock pair appears as specific to a given mainshock. These heterogeneities can be due to the triggering mainshock characteristics and/or to the local geological and weathering conditions. From the analysis of the five sequences, we observe that the two surface-rupturing earthquakes (Chi-Chi and Kashmir earthquakes) display different distance distribution patterns than the three buried earthquakes. For distances less than $L/2$, the two surface-rupturing earthquakes triggered relatively more aftershocks and landslides than the buried-rupturing earthquakes. In addition, for distances less than $0.2L$, there is a plateau of the number of aftershocks for distances calculated to the surface fault trace for the two surface-rupturing earthquakes. For the three buried earthquakes, and for distances calculated to the inferred surface fault trace, the number of aftershocks first increase with distance and then decreases for distance larger than the mainshock fault length. These differences suggest that the mechanisms driving aftershock triggering may be different for surface-rupturing or buried earthquakes.

For distances larger than $L/2$, the two surface-rupturing earthquakes triggered landslides and aftershocks at shorter distance than expected from their magnitudes (Figs 3b and 4b). If aftershocks and landslides are triggered by coseismic ground motion, then this result is not in agreement with Pitarka et al (2009) who showed that surface-rupturing earthquakes generated weaker near-fault ground motion than buried earthquakes, while at larger distances the tendency was reversed. The local conditions appear to influence the landslide and the aftershock distance distributions. Indeed, the two end-members of the distance distributions, Kashmir and Rotoehu landslides and aftershocks are associated to drier than usual and higher than usual rain conditions, respectively (Figs 3 and 4). And yet the influence of rainfall in triggering both landslides and aftershocks has been demonstrated (see DeVita et al (1998) for a reference list on landslide triggering by rainfall and Muço et al 1999, Ogasawara et al 2002 and Hainzl et al 2006 for the influence of rainfall on earthquake triggering).

There is no linear scaling of the number of landslides with PGA for the Chi-Chi and Northridge sequences, unlike the linear scaling demonstrated between landslide density and PGA by Dadson et al (2004) and Meunier et al (2007). We find that the Chi-Chi PGD is the quantity that best explain the Chi-Chi landslide and aftershock distance distributions (Fig. 5).

In addition, the role of PGD and associated static stress changes is enhanced by the occurrence of most landslides and aftershocks on the hanging wall. Indeed, Ma et al (2005) showed that the maximum Coulomb stress changes (up to 2 bars) occurred on the hanging wall, for an idealized case of thrust for the Chi-Chi earthquake. Nevertheless, all Chi-Chi landslides and aftershocks are not located within the zone of positive Coulomb stress changes. In the same way, we can extrapolate the Chi-Chi idealized thrust model to the three other thrust sequences. Here also, not all landslides and aftershocks are situated within the zone of positive Coulomb stress changes. Other mechanisms are known to influence landslides and aftershocks triggering. We already mentioned dynamic triggering, especially for the landslides occurring more than one time the ruptured fault length. Another phenomenon known to enhance landslide failure is site amplification. For instance, Sepulveda et al (2005) showed that the observed extensive rock sliding and falling at Pacoima Canyon, triggered by the Mw=6.6 Northridge mainshock, would not have been possible in the absence of seismic waves amplification.

Publication

Tatard, L and Grasso, Unified picture for aftershocks and earthquake-triggered landslides, in preparation for J.G.R, 2010.

References

- S.J. Dadson, N. Hovius, H. Chen, W.B. Dade, J.C. Lin, M.L. Hsu, C.W. Lin, M.J. Horng, T.C. Chen, J. Milliman, et al. Earthquake-triggered increase in sediment delivery from an active mountain belt. *Geology*, 32(8):733, 2004.
- P. De Vita, P. Reichenbach, J.C. Bathurst, M. Borga, G. Crosta, M. Crozier, T. Glade, F. Guzzetti, A. Hansen, and J. Wasowski. Rainfall-triggered landslides: a reference list. *Environmental Geology*, 35(2):219-233, 1998.
- K.R. Felzer and E.E. Brodsky. Decay of aftershock density with distance indicates triggering by dynamic stress. *Nature*, 441(7094):735-738, 2006.
- J. Gomberg, P. Bodin, and P.A. Reasenberg. Observing earthquakes triggered in the near field by dynamic deformations. *Bulletin of the Seismological Society of America*, 93(1):118-138, 2003.
- S. Hainzl, T. Kraft, J. Wassermann, H. Igel, and E. Schmedes. Evidence for rainfall-triggered earthquake activity. *Geophysical Research Letters*, 33(19):L19303, 2006.
- P.A. Johnson and X. Jia. Nonlinear dynamics, granular media and dynamic earthquake triggering. *Nature*, 437(7060):871-874, 2005.
- D.K. Keefer. Investigating landslides caused by earthquakes - a historical review. *Surveys in Geophysics*, 23:573-510, 2002.
- K.F. Ma, C.H. Chan, and R.S. Stein. Response of seismicity to Coulomb stress triggers and shadows of the 1999 Mw=7.6 Chi-Chi, Taiwan, earthquake. *Journal of Geophysical Research - Solid Earth*, 110(5), 2005.
- P. Meunier, N. Hovius, and A.J. Haines. Regional patterns of earthquake-triggered landslides and their relation to ground motion. *Geophysical Research Letters*, 34(20):1- L20408, 2007.
- B. Muço. Statistical investigation on possible seasonality of seismic activity and rainfall-induced earthquakes in Balkan area. *Physics of the Earth and Planetary Interiors*, 114(3):119-127, 1999.
- H. Ogasawara, K. Fujimori, N. Koizumi, N. Hirano, S. Fujiwara, S. Otsuka, S. Nakao, K. Nishigami, K. Taniguchi, Y. Iio, et al. Microseismicity induced by heavy rainfall around flooded vertical ore veins. *Pure and Applied Geophysics*, 159(1):91-109, 2002.
- Y. Ogata and K. Katsura. Analysis of temporal and spatial heterogeneity of magnitude frequency distribution inferred from earthquake catalogues. *Geophysical Journal International*, 113(3):727-738, 1993.
- A. Pitarka, L.A. Dalguer, S.M. Day, P.G. Somerville, and K. Dan. Numerical Study of Ground-Motion Differences between Buried-Rupturing and Surface-Rupturing Earthquakes. *Bulletin of the Seismological Society of America*, 99(3):1521, 2009.

S.A. Sepulveda, W. Murphy, R.W. Jibson, and D.N. Petley. Seismically induced rock slope failures resulting from topographic amplification of strong ground motions: The case of Pacoima Canyon, California. *Engineering geology*, 80(3-4):336-348, 2005.

R.S. Stein. The role of stress transfer in earthquake occurrence. *Nature*, 402(6762):605-609, 1999.

D.L. Wells and K.J. Coppersmith. New empirical relationships among magnitude, rupture length, rupture width, rupture area, and surface displacement. *Bulletin of the Seismological Society of America*, 84(4):974-1002, 1994.

Figure captions:

Figure 1. Aftershock-mainshock (red curves) and landslide-mainshock (green curves) distance Probability Density Functions (PDF). Left: Distance to hypocenter, Middle: Distance to epicenter, Right: Distance to seismogenic fault through epicenter for the five events. The PDF were computed using a log binning and then convolved with a gaussian kernel, e.g. Izenman (1991).

Figure 2. Same as Figure 1 using a different measure of distance : Left: Distance to actual (Chi-Chi and Kashmir) or inferred (Fiordland, Northridge, Rotoehu) surface fault trace. Middle: Distance to actual or inferred surface fault trace, for the events on the hanging wall, bounded to the width of the ruptured fault length. Right: same than middle graphs, discrete distribution.

Figure 3. Distribution of aftershock distances. a) Distance to surface fault trace; b) Distance to surface fault trace normalised by the ruptured fault length. Red curve: Chi-Chi earthquake, green curve: Kashmir earthquake, blue curve: Fiordland earthquake, black curve: Northridge earthquake, cyan curve: Rotoehu earthquake.

Figure 4. Distribution of landslide distances. a) Distance to surface fault trace; b) Distance to surface fault trace normalised by the dimension of the earthquake, *i.e.* the ruptured fault length. Red curve: Chi-Chi earthquake, green curve: Kashmir earthquake, blue curve: Fiordland earthquake, black curve: Northridge earthquake, cyan curve: Rotoehu earthquake.

Figure 5. Aftershock density (red), landslide density (green) and ground motion (blue) as a function of hypocentral distance normalized by L for Chi-Chi (a-c) and Northridge (d-f) earthquakes. Ground motion is measured by PGA (left), PGV, (middle) or PGD (right).

Figure 1

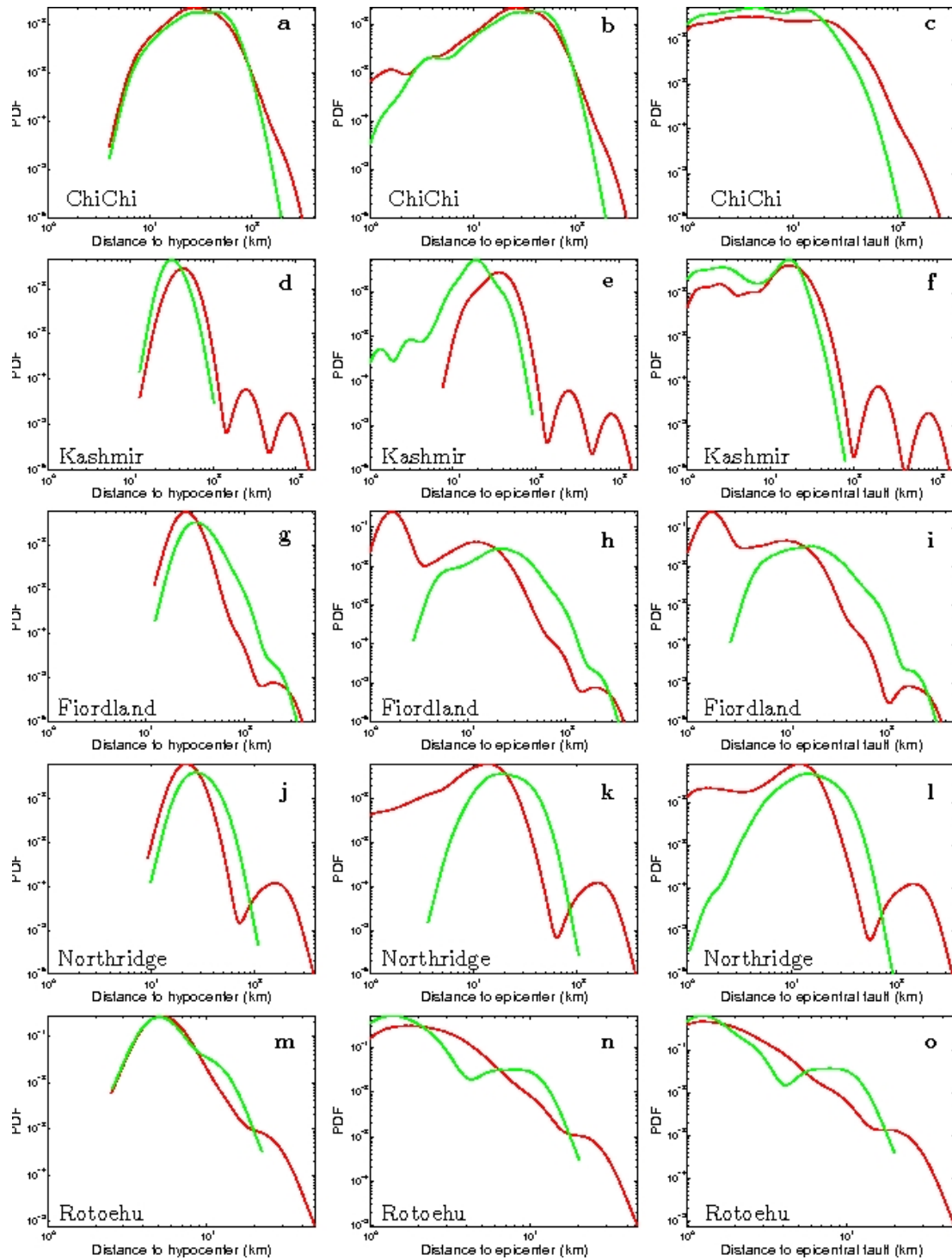


Figure 2

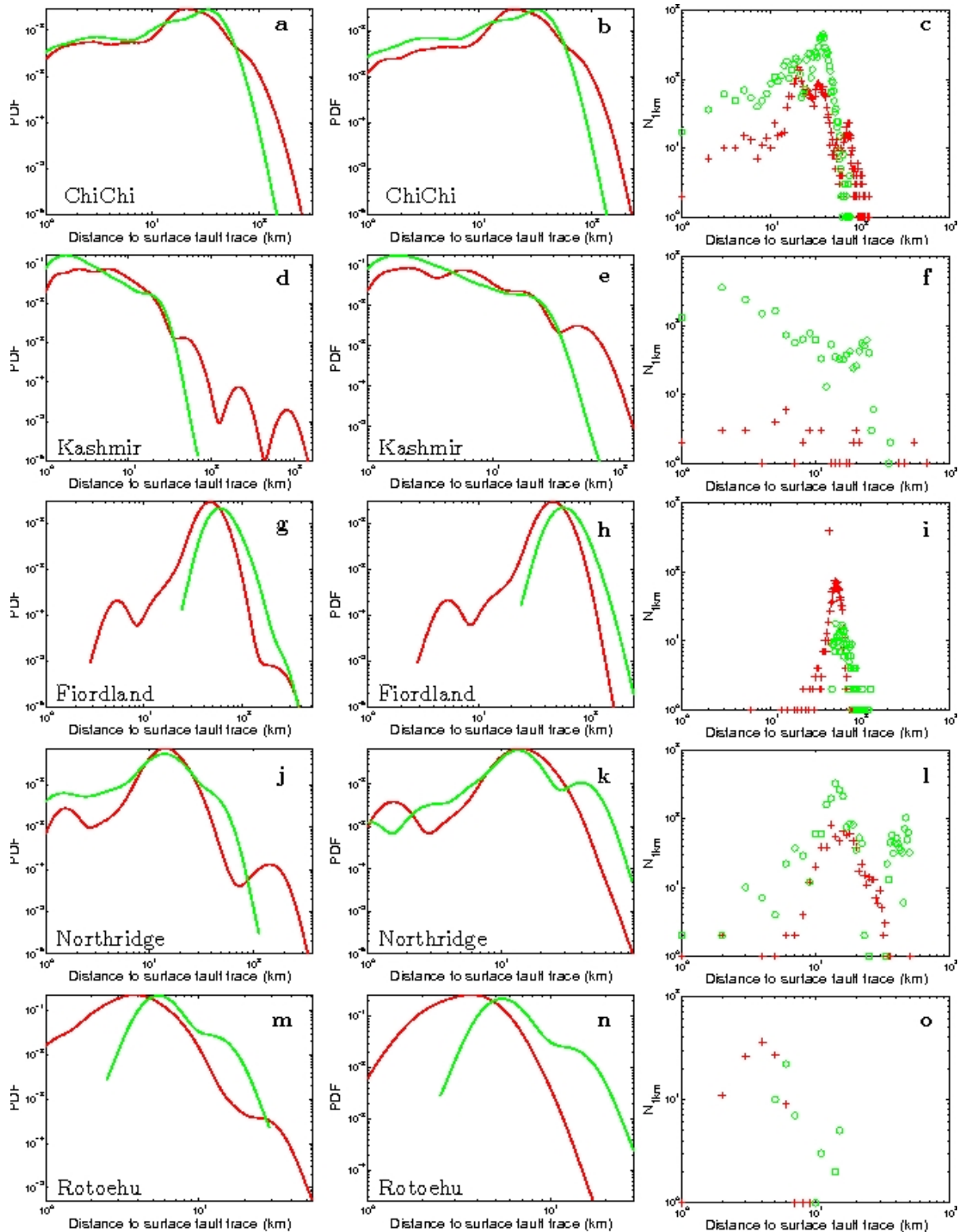


Figure 3

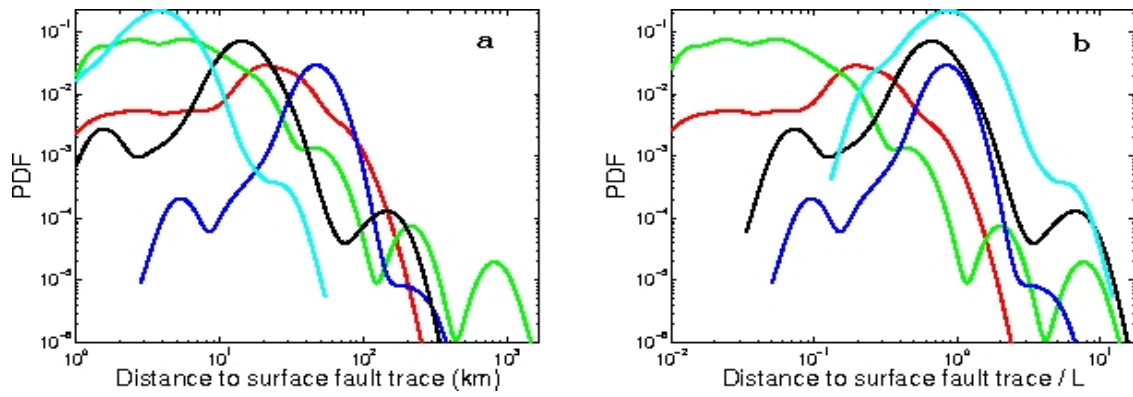


Figure 4

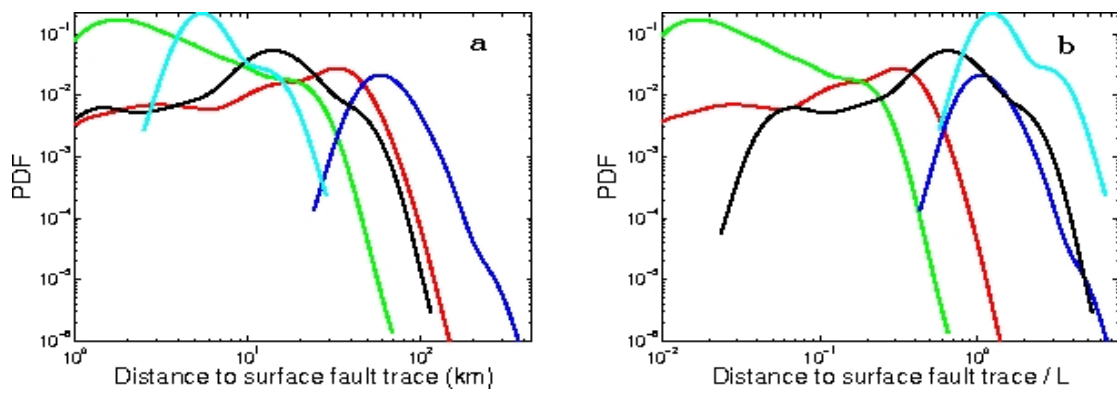


Figure 5

